Monitoring Strong Tidal Currents in Straits and Nearshore Regions

Alexei Sentchev, Max Yaremchuk and Maxime Thiébaut

Introduction

Open-ocean currents flow in complex patterns affected by wind, water density gradients, topography of the ocean floor, and the Earth's rotation. These large scale and relatively slow evolving forcing terms create water motions that are relatively persistent in magnitude and direction. In contrast, near-shore currents exhibit much stronger magnitude and variability both in space and time. Near the boundaries, in shallow water regions, and in narrow straits, flow dynamics is increasingly complex: tides and tidal currents are amplified, stratification effects are more pronounced, wind driven flows can contribute to extremely large variation of the sea level, while frictional effects in strong currents result in complex turbulent motions.

The strongest currents that can be experienced in coastal regions have tidal origin. Near the coast, tidal dynamics can be considerably modified by the shallow water and the coastline, and tidal current speed attains values of several meters per second that open ocean currents never reach. Regions of such high-tidal current speeds are sparse, and are typically the result of topographic flow amplification. A fast moving tide passing through a constriction can result in a tidal race (extremely strong current). It can also give rise to the formation of waves, eddies, and hazardous currents. In extreme cases, such as in Skookumchuck Narrows in British Columbia, through which tides can travel at more than 17 knots, very large whirlpools develop, which can be extremely hazardous to navigation. In other

A. Sentchev (✉) · M. Thiébaut
Lab. Oceanography and Geosciences, UMR 8187, LOG,
Université du Littoral - Côte d'Opale, CNRS, Université de Lille, Wimereux, France
e-mail: alexei.sentchev@univ-littoral.fr

M. Yaremchuk
Naval Research Laboratory, Stennis Space Center, Hancock, USA
e-mail: max.yaremchuk@nrlssc.navy.mil

M. G. Velarde et al. (eds.), *The Ocean in Motion*, Springer Oceanography,
https://doi.org/10.1007/978-3-319-71934-4_33

coastal areas, located in their majority along the UK and French coast, not so large but still impressive current speeds (more than 10 knots) are encountered.

Coastal ocean hydrodynamic models, routinely used for SSH and currents forecasting, are not always capable of resolving local bathymetric features and complex physics governing a fast moving tide. In such situations, monitoring of coastal currents by a bottom-based or towed current recording system remains a real but not unique opportunity. In turn, in situ observations by bottom-mounted Acoustic Doppler Current Profiler (ADCP) in strong tidal flows are very difficult to perform because they require highly qualified staff, boats, specific equipment, and if the survey is successfully conducted, the acquired data do not allow to characterize the spatial variability of the flow neither its long-term variation.

Underway velocity measurements by towed or vessel-mounted ADCP is another efficient tool for tidal flow characterization in nearshore areas. In the early studies [8, 32], velocity profiles were sampled with sufficient frequency while the vessel steamed around a circuit allowing to resolve the vertical structure of the tidal current and its spatial irregularities. Using broadband ADCP surveys Goddijn-Murphy et al. [9], Polagye and Thomson [18] documented fine scale velocity variations caused by tidal flow interaction with land and islands. However, the rapid change of the tidal flow during surveying period tends to induce errors in the velocity map interpretation. Goddijn-Murphy et al. [9] showed that the accuracy in reconstruction of the full 4-dimensional tidal flow can be significantly increased by merging observed velocities with the dynamical constraints provided by numerical models. More recently, Sentchev and Yaremchuk [25] used the optimal 4-dimensional interpolation technique for reconstructing space-time evolution of the velocity field derived from towed ADCP surveys in the Boulogne harbour (English Channel). This approach, which combines underway velocity measurements and modelling, offers a real opportunity for short-term monitoring of the strong nearshore circulation.

Another technique of coastal flow monitoring involves remote sensing of surface currents by High Frequency Radars (HFR). Although application of the HF radars in oceanography has more than 30-year history [17, 19, 26], its efficiency for monitoring powerful coastal flows, jets and tidal generated transient eddies was demonstrated only recently (c.f. [22]). A new interest for tidal current monitoring in straits and narrows is motivated by the growing development of the tidal energy conversion by in-stream devices. The UK was a pioneer in this field by installing the first commercial 1.2 MW tidal turbine in the Strangford Loch, a narrow strait connecting the inland tidal basin to the Irish Sea. In France, the Sabella Co. installed its first of three 0.5 MW tidal turbines in the Fromveur Strait (W. Brittany). Other projects aim to install tidal stream conversion systems at various sites in France (Alderney Race) or in Scotland (Pentland Firth). In this context, long term monitoring of strong tidal flows at these sites is of primary importance for engineering applications and assessing the tidal stream potential.

In this chapter we give an overview of the two prospective techniques for monitoring strong currents in the nearshore regions with high tidal stream potential: the remote sensing by HFRs, and underway measurements by a towed ADCP. In

the next section, we first consider the basic principles of HFR-based observations of surface currents and then describe application of the method for assessment of spatial and temporal variability of the tidal flows at two sites where powerful tidal currents dominate local circulation: off the western coast of France and in the Strait of Dover. In section "Measurements of Tidal Currents with a Towed ADCP System", we briefly describe a compact ADCP towing system and demonstrate its application in two regions (the Solent and Dover Strait) in the English Channel. In section "Summary", we summarize the results and discuss the prospects of using the techniques, in particular, for applications related to tidal energy conversion.

Monitoring Surface Currents with HF Radars

Basic principle High Frequency radars operate in a frequency band 5–45 MHz. A part of the electromagnetic energy transmitted at these frequencies is trapped in the "surface-wave" mode and remains bound to the sea surface, following the Earth curvature. Moreover, in this frequency band, the electromagnetic waves have wavelengths that are commensurate with wind-driven gravity waves on the ocean surface. The ocean waves whose wavelengths are exactly half as long as those of the broadcast radio waves are responsible for the resonant backscatter, an example of a phenomenon known as Bragg scattering. Crombie (1955) first observed that the peak energy of HF radio waves reflected from the sea surface occupies a narrow frequency range near the frequencies $\pm f_b$, called the Bragg frequency; f_b represents the Doppler shift of the backscattered signal above and below the HFR frequency, it is defined as $f_b = g/\pi\lambda$, where λ is the radar wavelength, g is the acceleration of gravity. These two Bragg peaks in the power spectrum are produced by the coherent scattering of the HFR waves by the Bragg sea surface waves travelling radially toward and away from the radar.

In an important early study, Stewart and Joy [26] observed that there are often small frequency differences between the observed Doppler shift of the backscattered HFR waves and the Doppler shift predicted from the surface gravity waves moving over still water. Using radar-tracked surface drogues to directly measure ocean currents, they showed that the observed differences resulted from surface ocean currents and that the current speed toward or away from the radar could be estimated. In particular, radial velocity v_r of the surface current (a projection of the current velocity vector on the radar beam) can be retrieved from the Doppler shift Δf of the observed Bragg peaks, compared to their theoretical values, by using the Doppler formula $v_r = \Delta f/2\lambda$.

These principles are the basis for the mapping of surface currents by oceanographic HFRs. Since then, many validation studies comparing HF radar-derived surface currents with in situ observations have contributed to the growing acceptance and use of HFRs for measuring surface currents (e.g., [4, 16, 21, 23]). Stewart and Joy [26] assumed that a HF radar samples vertically integrated current velocity. Earlier work by Kirby and Chen [12] and more recent studies [21, 23] allowed us to

validate this assumption experimentally and conclude that the HFR-derived velocity corresponds to exponentially weighted velocity profile and that the equivalent velocity value is found at the effective depth $z = \lambda/8\pi$. The effective depth is of the order of 0.75 m for 16 MHz and 2.3 m for 5 MHz radar.

Mapping the surface velocity field Individual radar samples the surface velocity over a large area which can extend up to 200 km offshore (5 MHz long-range radar). This area is divided into a number of directional beams and each beam contains a large number of bins (range cells). A good quality Doppler signal requires each range cell to be larger than at least 150 Bragg wavelengths. For this reason, the bin size becomes larger as the radar frequency decreases. A HFR cannot unambiguously identify the arrival directions of backscattered signals. Currently, HFR systems for mapping surface currents may be classified into two types, beam-forming (BF) and direction-finding (DF), based on the method used to determine arrival directions.

Beam-forming radars use a linear array of antenna elements that are steered by adjusting the amplitudes and phases of received signals (e.g., [27]). An early *beam-forming* (BF) radar, used extensively for mapping surface currents, was the ocean surface current radar (OSCR) [20] with an azimuthal resolution of 10°. More recently, the Wellen radar (WERA) was developed by Gürgel et al. [10] using beam-forming configurations with up to 16 antenna elements offering an azimuthal resolution of ~3–4°. Such an array often occupies more than 150 m of coastline which is not always practical.

To achieve smaller footprints, *direction-finding* (DF) configurations are used. These radars compare the phases and amplitudes of radio signals received by closely spaced antenna elements coupled with various direction-finding inversion algorithms. The most common direction-finding radar is the CODAR SeaSonde [1]. Both algorithms (DF and BF) can be used to identify the arrival direction by linear-array antenna WERA system. The azimuthal resolution produced by each method can play a crucial role in analysis of surface circulation patterns in the regions, where high horizontal velocity gradients are expected. Figure 1 provides an example of such a difference in spatial structure of current velocity sampled by 12.4 MHz WERA system around the Ushant Island, off the western Brittany coast of France, by using both DF and BF algorithms. The DF allows small-scale structures of tidal currents to be better resolved. On the contrary, DF radars often produce coverage gaps (cf. eastern and southern margin of the radar coverage area in Fig. 1).

A single HFR measures projection of the current velocity vector on the beam direction. Therefore, velocity measurements by at least two distant radars are required for reconstruction of the vector velocity map. At a point of the beam intersection of two radars, the east–west (u) and north–south (v) components of the surface current vector may be found by solving a system of two equations involving measured radial velocities and known beam angles. If a point on the sea surface is in the coverage area of three or more radars, then u and v can be obtained from a least-squares solution of the corresponding system of linear equations. These are the

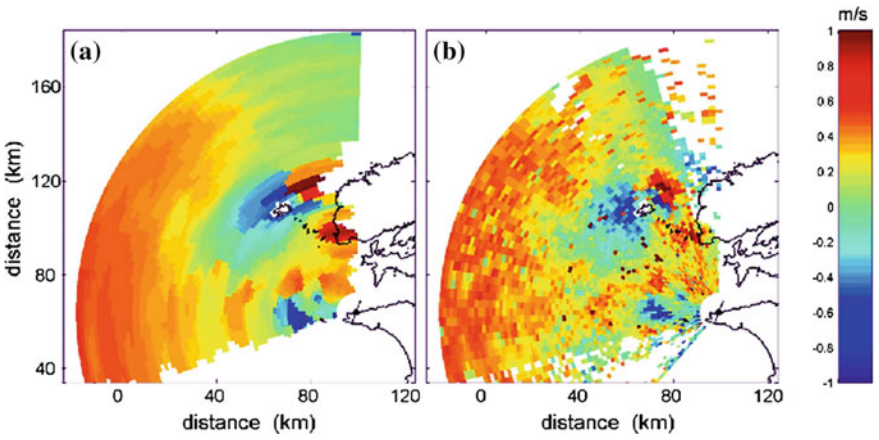

Fig. 1 Radial velocities of surface currents retrieved by the DF (**a**) and BF (**b**) algorithms from HF radar measurements off the W. Brittany coast

methods of local reconstruction of the velocity field. More sophisticated global interpolation methods use linear combinations of radial velocities at all measurement points in conjunction with additional kinematic and/or dynamical constraints to reconstruct the entire velocity field (e.g., [11, 33, 34]).

The Open-boundary Mode Analysis (OMA) method of Kaplan and Lekien [11] performs an expansion of the interpolated velocity field in the eigenfunctions of the 2D Laplacian operator in the interior of the domain with the additional control at the open boundaries by the eigenfunctions of the 1D Lapalcian.

Yaremchuk and Sentchev [33] proposed a more general and versatile 2D variational method of interpolation (2dVar) based on the direct minimization of the cost function with respect to the interpolated velocity field $\mathbf{v}(\mathbf{x})$. Apart from attracting $\mathbf{v}$ to the available observations, the cost function penalizes high-frequency components of the curl and divergence of $\mathbf{v}(\mathbf{x})$. This feature can help to overcome some limitations related to a lack of data. Additional smoothness of the interpolated field is enforced by penalizing the squared Laplacian of velocity, thus providing the algorithm with flexibility and efficient noise control. Kinematic constraints (zero flux on rigid boundary) incorporated into 2dVar, appear particularly useful in regions complicated topography. Yaremchuk and Sentchev [34] also developed a gap-filling technique for HFR observations based on the EOF analysis of the observational errors. In the subsequent presentation, the 2dVar interpolation scheme developed by the authors was used for the reconstructing the velocity fields.

HFR observations in the English Channel In this section, we describe applications of the long-term monitoring technique by HFRs in two regions where implementation of traditional in situ observational platforms is difficult due to extremely strong tidal currents or due to busy shipping traffic, economic and environmental constraints.

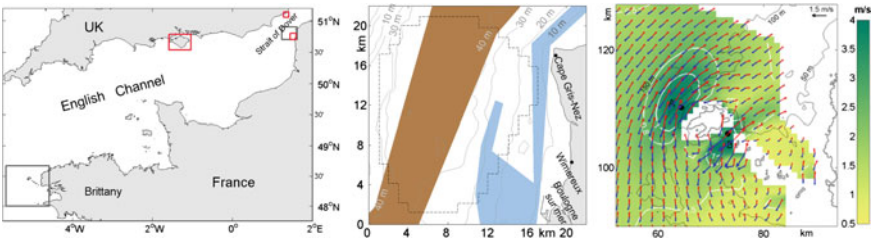

Fig. 2 Left: The English Channel (left) and areas covered by HFR (gray rectangles) and towed ADCP (red rectangles) velocity observations. Middle: HFR coverage zone (gray dashed line) off the Opal coast of France. The HFR sites are shown by black dots. The navigation routes of vessels and fishing areas are shown by brown and blue shading respectively. Contour interval of the bathymetry is 10 m (grey solid lines). Right: Study area off the W. Brittany coast (in the Iroise Sea) with radar coverage zone (grey shading) and radar sites (grey circles). Contour interval of the bathymetry is 50 m (black solid lines)

The first region is located in the Dover Strait off the Opal coast of France, where tidal amplitude can be as high as 9 m and currents can reach 3 m/s. The site is relatively shallow water with depth less than 50 m. In the middle of the Strait, there are sandbanks oriented alongshore (Fig. 2). Currents are predominantly semidiurnal with a pronounced fortnightly modulation due to the interference of the M_2, S_2, and N_2 tidal constituents. In May–June 2003, two Very High Frequency radars (VHFR) were deployed for a 35-day period to monitor tidal currents. Radar sites were located on the Cape Gris Nez and in Wimereux, 12 km southward (Fig. 2). The radars were operating at frequencies 45 MHz and 47.8 MHz, and measured velocities over a distance up to 25 km offshore at 600 m radial and 10° azimuthal resolution, with time discretization of 20 min. The radial velocities measured by the two radars were interpolated on a regular grid with 1 km spacing by variational method with the gap filling capability. As a result, one month long sequence of current velocity maps was generated and used for assessing tidal circulation in the French sector of the Dover Strait [24].

The second study site is located at the entrance to the English Channel, off the western Brittany coast of France, and has larger extension (Fig. 2). The bottom topography is complicated by the group of small islands, islets, and rocks of the Molène archipelago separated from the mainland by more than 15 km wide strait. The larger Ushant Island is separated from the Molène Islands by the 2 km wide and 60 m deep Fromveur Strait. Tidal currents in the strait are very strong with velocities often exceeding 4 m/s.

Two high-frequency Wellen Radars (WERA) operating at 12.4 MHz have been permanently operating on the W. Brittany coast since July 2006. Individual radar sites are located at Cape Garchine (site G), and Cape Brezellec (site B) (Fig. 2). The HFRs were configured to measure velocity in the surface layer 1 m thick at 1.5 km radial and 2° azimuthal resolutions, with a temporal resolution of 20 min. Radial velocities were interpolated on regular 1 km grid using 2dVar interpolation technique. The accuracy of the radar-derived velocities has been estimated by SHOM

(Oceanographic Division of the French Navy) through a comparison with surface drifters and ADCP current measurements for a period of 7 months. In the majority of situations, the discrepancy in velocity measured by different instruments did not exceed 0.15 m/s. A detailed description of the experimental settings, the methods of HFR data processing in the Iroise Sea can be found in Sentchev et al. [22].

Tidal current dynamics off the W. Brittany coast Velocity time series derived from HF radar measurements during the period 04/2007–09/2008 were used for assessing tidal circulation around Ushant Island and estimating the major properties of the flow. The maximum sustained velocity represents the maximum current observed. Tidal flow asymmetry accounts for the asymmetry of velocity magnitude during the tidal cycle. This imbalance between the strength of flood and ebb current speeds is quantified as: $a = \langle V \rangle_{flood} / \langle V \rangle_{ebb}$, where brackets denote time averaging of velocity values on flood and ebb flow respectively. The principal component analysis (PCA) [31] technique was applied to determine the principal direction of the flow during the ebb and flood tide phases. The direction asymmetry $\Delta\theta$ shows deviation of the flow from a straight line (dominant direction). This metric is defined as: $\Delta\theta = |\theta_{flood} - \theta_{ebb} - 180°|$. Current velocity spectrum was also estimated. It can help to explain the interaction between the principal tidal constituents resulting in a strong distortion of the velocity curve.

Spatial variability of tidal currents is quantified by assessing the axes of the tidal current ellipses derived from the PCA (Fig. 3). The length and orientation of ellipse's axis provide information about the tidal current strength and direction of flood and ebb flow and indicate the regions with the most powerful flow. The maximum and time averaged current velocity distribution shows significant spatial variations in the range from 0.75 to 4 m/s for the maximum velocity (Fig. 3, colour shading) and from 0.5 to 2 m/s for the mean spring tide velocity (Fig. 3, white

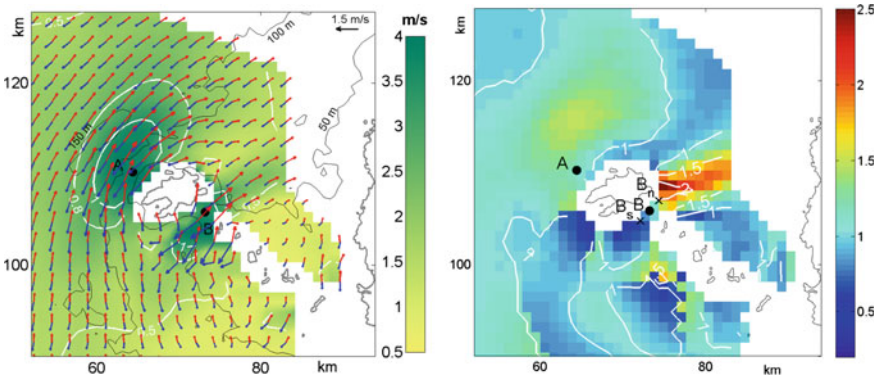

Fig. 3 Left panel: Radar derived current velocities of the flood (red) and ebb (blue) flow during spring tide conditions. Time average and maximum surface current velocity during the study period are shown by white contours and color shading respectively. Black circles mark location of grid points where the maximum velocities are observed (locations A and B). Right panel: Current velocity asymmetry a. B, B_n, B_s mark locations used for the analysis of current velocities

contours). The strongest currents are identified in two areas: west of Ushant Island and in the Fromveur Strait (locations A and B in Fig. 3). Bathymetry gradients and the presence of islands cause flow acceleration, tend to tighten the streamlines and provide the maximum velocities in these two sectors.

Figure 3 also shows a significant (up to 90°) misalignment in the current direction during flood (red) and ebb tide (blue arrows) in the eastern and southern sectors of Ushant Island. Such a deviation of the flow during a tidal cycle is known as direction asymmetry. Sentchev et al. [22] documented the presence of transient eddies in these areas which might explain such a large difference in the direction of the ebb and flood flow. In the north-western sector of the domain, $\Delta\theta$ ranges from 0° to 10°, indicating that ebb and flood flows are mostly aligned.

Another interesting feature of the tidal dynamics around Ushant Island is the velocity asymmetry *a*. The asymmetry varies in a wide range, from 0.5 to 2.5, and shows a large spatial pattern with $a > 1$ in the west and $a < 1$ in the south (Fig. 3). The strongest variation of asymmetry is observed in the Fromveur Strait. Here, the asymmetry attains 2.5 in the onshore sector, indicating that flood flow velocities are by far larger than the ebb flow velocities. The asymmetry decreases toward the centre of the strait (point B in Fig. 3), where the tidal flow reaches a balance ($a = 1$). Abrupt changes in the flow regime occur at very short distance in the strait. The asymmetry values reveal very strong variation, from 1.9 to 0.8, between two locations, B_n and B_s, separated by only 2.5 km at either side of the centre of strait (location B). This gives flood flow velocities up to 2 m/s larger than ebb flow velocities in B_n, and ebb flow velocities larger by ~1 m/s in B_s. Such a strong asymmetry variation, to the best of our knowledge, has never been documented elsewhere.

Different properties of the tidal flow in nearshore environment can explain asymmetry variations. Non-linear interactions between the principal semi-diurnal constituents yield overtides and compound tides. It was established, that the phase difference between semidiurnal and quarter-diurnal tidal constituents governs the tidal flow asymmetry. In particular, the following relationship can be used to diagnoze tidal asymmetry: $\gamma = 2\Phi_{M2} - \Phi_{M4}$, where Φ_{M2} and Φ_{M4} are the phases of the M_2 and M_4 tidal current constituents [6]. Tidal current curve is symmetric when $\gamma = 90°, 270°$. Maximum asymmetry is achieved at $\gamma = 0°, 180°$.

Harmonic analysis of velocity time series in the Fromveur Strait revealed the presence of overtides and compound tides in the spectra. In the central point of the strait (point B), the value of γ was ~270°, thus indicating that the velocity curve is balanced here ($a \approx 1$). On the contrary, in the onshore and offshore sectors of the Strait, the value of γ is close to 215° and 200° respectively, thus providing extreme asymmetry values and a large imbalance of the current flow [29]. Non-linear interactions between the principal semi-diurnal constituents generate residual currents which also contribute to tidal flow asymmetry.

Tidal currents in the Dover Strait The spatial variability of tidal currents in the southern sector of the Dover Strait are quantified using parameters of synthesized tidal current ellipses (Fig. 4) derived from the PCA. Spring tide period (May 16,

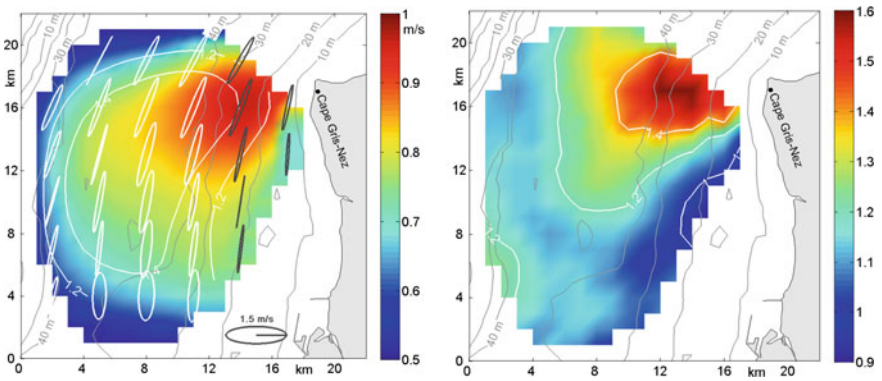

Fig. 4 Left panel: Mean surface current velocity (m/s) during the study period (color) and during the spring tide period in May 2003 (white contours). Shown also tidal current ellipses derived from PCA on May 16, 2003 (every third ellipse is shown). Black white ellipses denote counter-clockwise and clockwise rotating currents. Right panel: Current velocity asymmetry a

2003) was selected to illustrate the location and magnitude of the strongest currents observed. The ellipse orientation shows that the tidal currents are controlled by the topography, producing alignment of the semi-major axes along the depth contours. Anisotropy in current velocity field with a relatively high ellipticity is observed over the sandbanks, in the middle and in the southern part of the study domain. Two distinct zones with opposite sign of current vector rotation are clearly identified (black and white ellipses). They are separated by a line roughly following the 30-m isobath. This suggests that tidal currents are alternatively divergent or convergent during the current reversal. The time averaged current velocity distribution shows low spatial variations with values ranging from 0.5 to 1 m/s, with the highest velocity observed off the Cape Gris Nez. The maximum current speed observed by the radars does not exceed 2 m/s in the study site. The current asymmetry a exceeded unity in almost entire domain, indicating the flood flow dominance (Fig. 4). The maximum current asymmetry ($a = 1.6$) is observed 6 km west of the Cape Gris Nez, indicating the effect of the cape on the spatial distribution of phase and amplitude of the principal (M_2) tidal constituent and its higher order harmonics (M_4, MS_4).

Measurements of Tidal Currents with a Towed ADCP System

Although HFRs provide an efficient tool for long-term monitoring of tidal currents on a larger scale, their spatial resolution could be insufficient for many practical applications, such as identifying precise location of free-stream tidal turbines at tidal energy sites. Much higher spatial resolution can be provided by ship-borne ADCP

observations. In contrast to the bottom-mounted or moored ADCPs, this method of surveying does not require deployment of numerous instruments to obtain adequate spatial resolution and it is not vulnerable to harsh environmental conditions and extreme tidal velocities. Extensive ADCP surveys demonstrated that tidal currents are characterized by significant variations at the scales of a few hundred meters [9, 14], and thus, require a very high resolution surveying during multiple tidal cycles. At the same time, finite speed of the surveying vessel imposes certain limitations on the accuracy of reconstruction of the 4-dimensional velocity field. To resolve the issue, observed velocities should be constrained by the relationships governing tidal dynamics.

This approach was pursued by Goddijn-Murphy et al. [9], who synthesized vessel mounted ADCP transects in the Pentland Firth (Scotland) with the output of the Orkney 2D tidal Model (ORKM) and obtained snapshots of the currents during different tidal phases. Recently, Sentchev and Yaremchuk [25] proposed a 4D optimal interpolation (OI) technique for processing underway velocity measurements. The method employs statistics of a tidal model to infer the velocity error covariances required by the interpolation algorithm.

In this section, we discuss the results of high resolution current mapping with a towed ADCP at two sites in the English Channel characterized by strong tidal currents. They are of certain interest for industrial companies developing energy conversion systems, and thus require extended assessment of the local hydrodynamics.

Methodology High resolution current mapping is performed using an experimental platform carrying a broadband ADCP (1200 kHz or 600 kHz Teledyne RDI WorkHorse Sentinel) towed by a light boat (Fig. 5). The distance from the boat is controlled by an adjustable side fin allowing to keep the platform at a side of the boat and thus to avoid contamination of the observed velocities by the wake. Two additional rear fins installed on the hulls assure stability of the forward propulsion. The ADCP is set to operate at a pinging rate of 1 Hz providing one velocity profile per second with an accuracy of 0.05 m/s. The velocities are sampled with 0.5 m vertical resolution; the first bin centred at 0.75 m. Bottom tracking enables to correct for boat's movement and the recorded velocities form a current vector in the fixed frame relative to the bottom.

The boat speed typically varies within 2–4 m/s during a survey. The recorded ADCP data are merged with high resolution GPS data. The geolocalisation system GENEQ SXblue, mounted on the side of the platform (Fig. 5) and operating at 1 Hz, provides positioning accuracy of 40–80 cm at towing speeds of 2–4 m/s. The above described system, called Koursk, was used for high resolution current mapping at two perspective sites of marine renewable energy in the English Channel: in the Solent and off the Dover harbour.

Assessment of tidal dynamics in the Solent and off the Dover harbor Tidal motions in the Solent (Fig. 5, right panel) are very complex and well known for the unusual phenomena such as the "Double High Water", the "Young Flood Stand", and the short duration of the ebb tide. These peculiarities result from a deformation

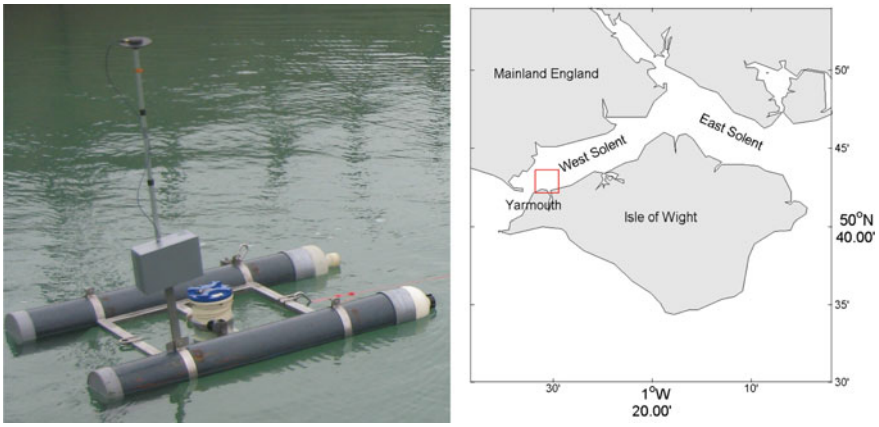

Fig. 5 Left panel: The experimental towing platform Koursk with ADCP profiler (in the centre), high precision GPS with GPS antenna and data acquisition module. Right panel: The Solent and the area covered by towed ADCP surveys in the West Solent (red rectangle)

of the tidal wave travelling through the Solent, generation of overtides and compound tides [3].

A total of five towed and one fixed point ADCP surveys were performed in July and October 2015 to assess the circulation in the West Solent in an area of approximately 3.5 km^2 at 100 m horizontal resolution (Fig. 6). Each survey lasted 1–1.5 h and covered different stages of a tidal cycle. The transects were oriented roughly in the south-north direction and separated by approximately 500 m. Figure 6 (left top panel) shows an example of the surface current velocities recorded by the system during the spring flood tide, one hour before High Water (HW) in Southampton. Significant spatial variations of velocity are observed with a local current intensification in the southwestern and northeastern sectors with steeper bottom topography. The highest current speed, ranging from 2.5 to 3 m/s, was recorded there both on ebb and flood tide. High resolution mapping allowed identifying small scale features of tidal circulation. These include a slacking current in the vicinity of the Yarmouth harbour and in the shallow northern sector, and a transient anticyclonic eddy, 0.5 km in diameter in the southern part of the surveyed zone. The eddy is generated during the flood flow by bottom friction in the vicinity the Sconce Point, which induces negative vorticity downstream.

The towed ADCP survey made possible assessing current variations with depth. Velocity distribution on a cross-section in the western part of the study area on flood flow shows the location of the tidal jet (Fig. 6, bottom panel). Large horizontal gradients of current speed are observed in the southern part of the westernmost cross-section. Velocity profiles appear rather homogeneous throughout the water column with the exception of the relatively thin boundary layer where the vertical velocity shear is large.

Typical flood tide velocities south of the Dover Harbor are shown in Fig. 6 (top right panel). A total of five towed ADCP surveys were performed during three days in July and September 2014 here. The current speed is higher all over the domain

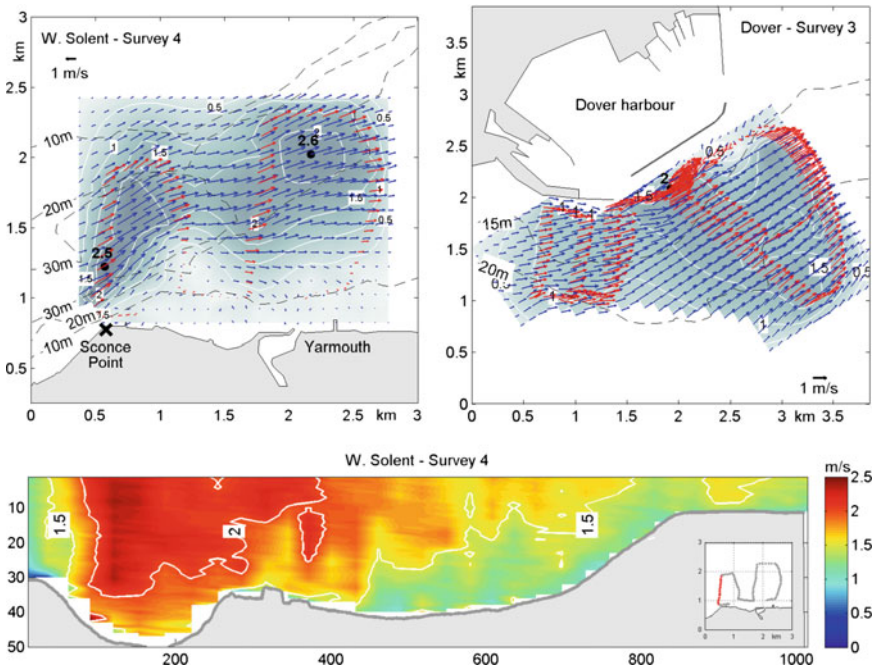

Fig. 6 Surface layer velocities in the West Solent during spring flood tide on 16-10-2015, one hour before HW in Southampton (top left) and off the port of Dover during mean flood tide on 5-7-2014, 2.5 h after LW in Dover (top right). Current vectors derived from underway ADCP velocity measurements, 30-s averaged, are shown in red. Bottom panel: Current speed over the cross-section in the West Solent during ebb tide on 1-9-2014. Cross-section location is given in red in the insert

during flood tide than during ebb tide, but the flow pattern looks similar. As can be expected, tidal currents are generally constrained by shoreline, port dykes, and bathymetry contours. Highest velocities are found in the vicinity of the breakwater, and then gradually decrease seaward. A small size cyclonic vorticity feature is identified in the northeastern part of the domain. It indicates the presence of a large recirculation area with relatively weak currents east of the breakwater.

4D interpolation of the underway velocity measurements Uncertainties in spatial patterns of the tidal flow reconstructed under the assumption of instantaneous observations can be significant since evolutions of tidal currents at time scales of a few hours are often comparable to the surveying period. To avoid distortion of the results caused by temporal variation of the tidal flow during the survey, very short (20–30 min) transects are repeatedly made, usually around the peak tidal flow (e.g., [5]). This time limitation prevents continuous studies of larger domains, which require surveying times comparable with the characteristic time scale of the velocity field ($T \sim 2$–4 h).

In this section we present 4D optimal interpolation technique, in both space and time, allowing retrieving the entire evolution of tidal currents from the survey data. The technique employs tight space-time correlations in the tidal flow field that can be accurately simulated by the existing state-of-the-art numerical models. A brief description of the method and its application to assessing tidal circulation in a limited size area (Boulogne Harbour) are given below. The harbour is located in the French sector of the Dover Strait, in the vicinity of the area covered by the HFR observations (Fig. 2).

A straightforward method of statistically consistent spatial interpolation of a vector field is the well-known optimal interpolation (OI) pioneered by Gandin [7]. Since then, the approach was widely adopted in geosciences (e.g., [2, 30]). The OI technique can be easily extended to include time dimension by using the space-time correlation functions. In this approach, the optimal correction to the evolution of a background vector field $\boldsymbol{u}^m(\boldsymbol{x}, t)$ defined on a regular (model) grid is represented by a linear combination of the weighted differences between the background trajectory and the observed velocities. The weights a_i are chosen so as to minimise the mean square difference between observations $\boldsymbol{u}_i^*$ and the background field values $\boldsymbol{u}^m$, interpolated into the space-time locations of the observations by the (linear) operator $\boldsymbol{H}^i$, projecting gridded velocity values onto the i-th observation point from the apexes of the enveloping grid cell:

$$J_u = \left\langle \left[u^m + \sum_i \mathrm{a}_i (H^i u^m - u_i^*) \right]^2 \right\rangle \rightarrow \min(\mathrm{a}_i) \tag{1}$$

Here, angular brackets denote the statistical (ensemble) average, and summation is made over all (distributed in space and time) velocity values measured during the survey period. Given the space-time covariance matrices of the model $\boldsymbol{B} = \langle \boldsymbol{u}^m(\boldsymbol{x}, t)\, \boldsymbol{u}^m(\boldsymbol{x}', t') \rangle$ and observations $\boldsymbol{R}_{ij} = \langle \boldsymbol{u}_i^* \boldsymbol{u}_j^* \rangle$, and assuming that observation errors are not correlated with the model (background) errors, the OI interpolation formula takes the form:

$$u_{opt} = u^m + \sum_{ij} B H_j^T (H_i B H_j^T + R_{ij})^{-1} (H^i u^m - u_i^*) \tag{2}$$

In order to apply Eq. (2) for interpolating the surveyed velocities, $\boldsymbol{u}^m(\boldsymbol{x}, t)$ and $\boldsymbol{B}$ are specified using the output statistics from the regional model MARS-3D [13] configured for high resolution simulations in the surveyed area [25].

The result of interpolation allows accurate tracking of the motion of the anti-cyclonic eddy derived from underway velocity measurements by towed ADCP within the Boulogne harbor on March 27, 2012 (Fig. 7a). Figure 7 also shows two snapshots of the velocity field: 20 min after the beginning of the survey, at HW − 1.2 h, and at the end of the survey, at HW + 0.5 h. As it can be seen, the optimal interpolation enables relatively accurate assessment of the circulation pattern: at the beginning of the period (Fig. 7b), the eddy center was located just south

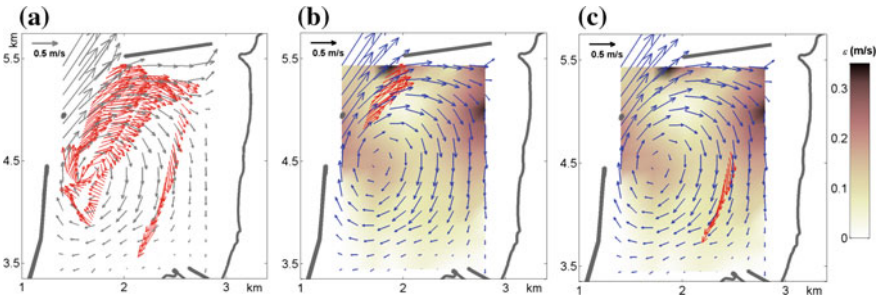

Fig. 7 **a** Observed (red) and modelled (gray) surface velocity fields during the towed ADCP surveys in Boulogne Harbour on March 27, 2012 1200–1400 GMT. Evolution of the anticyclonic eddy from HW − 1.2 h (**b**) to HW + 0.5 h (**c**). Red arrows show 30-s averaged ADCP velocities recorded along the track for the respective tidal stages. Blue arrows show interpolated velocities. Background shading shows the difference between the survey velocities interpolated in space and time and model velocities at mid-time of the survey

of the harbor entrance, 300 m east of the western seawall. In the northern part, the water inflow is observed with mean velocities ranging from 0.5 to 1 m/s. Later, at HW + 0.5 h, the eddy migrated northeastward and expanded in size to occupy the entire area of the harbor (Fig. 7c). The background color in Fig. 7 indicates the difference in the velocity magnitude between the space-time interpolated currents and the respective currents of the background model run $\boldsymbol{u}^m(\boldsymbol{x}, t)$. Most of the data-induced changes are observed in the northern part of the harbor with the major difference (≈0.30 m/s) at the periphery of the eddy, showing significant modifications of the circulation pattern provided by the interpolation.

Summary

Currents of several meters per second can never be experienced in the open ocean but could be encountered in straits and nearshore regions due to the interaction of tidal waves with topography. Although regions of such extreme currents are sparse, in situ observations of local flows are very difficult to perform due to extreme environmental conditions. Static velocity measurements performed by either bottom-mounted or moored ADCPs do not allow to adequately characterize neither the spatial structure of the flow nor its long-term variation. In this chapter, we presented two complimentary flow monitoring techniques that could be suitable for continuous observations of the extreme currents.

The first type of reported observations was provided by two HFR networks operated along the French coast, in the western and eastern sectors of the English Channel. The HFR-derived velocities of surface currents were analyzed by means of various numerical and statistical techniques. In particular, processing long-term HFR observations in the W. Brittany provided maps of surface currents in

unprecedented detail due to the application of the DF technique in conjunction with variational 2dVar interpolation. The approach was essential for accurate assessment of circulation around the islands and in the straits were high horizontal velocity gradients occur.

Our analysis revealed velocities exceeding 4 m/s and a pronounced asymmetry between the flood and ebb flow varying in a wide range, 0.5–2.5, around Ushant Island. The strongest variation of asymmetry was found in the Fromveur Strait. Neill et al. [15] investigated spatial variation of asymmetry around the Orkney Islands, where strong tidal currents occur, and documented the values ranging from 0.7 to 1.3. Four times larger asymmetry variation has been found around Ushant Island, which, to the best of our knowledge, has never been documented at any other place in the World Ocean.

HFR velocity monitoring in the Strait of Dover documented the strongest currents (up to 2.5 m/s at spring tide) occurring west of the Cape Gris Nez. This highly energetic area (power density ~1 kW/m^2), located outside the northward navigation routes and fishing zone, appears suitable for testing energy conversion devices there [28].

Although HFR-based observations present an adequate tool for monitoring extreme currents at larger scale, their spatial resolution is often insufficient for the task of accurate deployment of tidal turbines. In that respect, the presented high resolution current mapping system Koursk can be seen as complementary to other coastal observing systems, such as HFRs and moored ADCP arrays. The system was successfully tested in several sites (the Solent, ports of Dover and Boulogne) demonstrating a good combination of accuracy, portability and low cost of surveying. The system is equipped with an interpolation algorithm, which allows reconstructing space-time evolution of the velocity field for surveys whose duration is comparable or larger than the time scale of tidal variability (1–2 h).

Application of the technique in Boulogne Harbor demonstrated significant (30–60%) reduction of the model-data misfit for the velocity field obtained as a result of space-time optimal interpolation. Although the method was applied to recover surface circulation, it can be extended for assessment of the full 4D tidal flow dynamics using the data recorded throughout the entire water column. We believe that the proposed current mapping system may advance understanding and assessing coastal circulation in tidal environments, especially when used in combination with moored ADCP and/or HFR observations. The data acquired by HFRs and towed ADCP, combined with the presented methodologies of their processing could improve the efficiency of ongoing tidal energy conversion projects in France and UK. The HFR data can be also used for numerical model validation and for data assimilation in numerical models, which may improve their forecast capability.

Acknowledgements The authors acknowledge the support of the Interreg IVB (NW Europe) "Pro-Tide" project and support from the US Office of Naval Research. We also acknowledge the Oceanographic Division of the French Navy (SHOM) for providing ADCP and HF radar data in the Iroise Sea. The authors thank skipper Eric Lecuyer (LOG) and also Philippe Forget and Yves Barbin (MIO, Toulon) for their contribution to radar data processing.

References

1. Barrick, D. E. (2008). 30 years of CMTC and CODAR. In *IEEE/OES 9th Working Conference on Current Measurement Technology, 2008. CMTC 2008* (pp. 131–136). IEEE.
2. Bretherton, F. P., Davis, R. E., & Fandry, C. B. (1976). A technique for objective analysis and design of oceanographic experiments applied to MODE-73. In *Deep-Sea Research and Oceanographic Abstracts* (Vol. 23, pp. 559–582). Elsevier.
3. Dyer, K. R., & King, H. L. (1975). The residual water flow through the Solent, South England. *Geophysical Journal of the Royal Astronomical Society, 42*(1), 97–106.
4. Emery, B. M., Washburn, L., & Harlan, J. A. (2004). Evaluating radial current measurements from CODAR high-frequency radars with moored current meters. *Journal of Atmospheric and Oceanic Technology, 21*(8), 1259–1271.
5. Evans, P., Mason-Jones, A., Wilson, C., Wooldridge, C., O'Doherty, T., & O'Doherty, D. (2015). Constraints on extractable power from energetic tidal straits. *Renewable Energy, 81,* 707–722.
6. Friedrichs, C. T., & Aubrey, D. G. (1988). Non-linear tidal distortion in shallow well-mixed estuaries: a synthesis. *Estuarine, Coastal and Shelf Science, 27*(5), 521–545.
7. Gandin, L. S., & Hardin, R. (1965). *Objective analysis of meteorological fields* (Vol. 242). Israel Program for Scientific Translations. Jerusalem.
8. Geyer, W. R., & Signell, R. (1990). Measurements of tidal flow around a headland with a shipboard acoustic Doppler current profiler. *Journal of Geophysical Research: Oceans, 95* (C3), 3189–3197.
9. Goddijn-Murphy, L., Woolf, D. K., & Easton, M. C. (2013). Current patterns in the inner sound (Pentland Firth) from underway ADCP data. *Journal of Atmospheric and Oceanic Technology, 30*(1), 96–111.
10. Gurgel, K. W., Antonischki, G., Essen, H. H., & Schlick, T. (1999). Wellen Radar (WERA): A new ground-wave HF radar for ocean remote sensing. *Coastal Engineering, 37*(3), 219–234.
11. Kaplan, D. M., & Lekien, F. (2007). Spatial interpolation and filtering of surface current data based on open-boundary modal analysis. *Journal Geophysical Research, 112,* C12007.
12. Kirby, J. T., & Chen, T. M. (1989). Surface waves on vertically sheared flows: approximate dispersion relations. *Journal Geophysical Research, 94*(C1), 1013–1027.
13. Lazure, P., & Dumas, F. (2007). An external-internal model coupling for a 3D hydrodynamical model for applications at regional scale (MARS). *Advances in Water Resources*, *31*, 233–250.
14. Li, C., Armstrong, S., & Williams, D. (2006). Residual eddies in a tidal channel. *Estuaries and Coasts, 29*(1), 147–158.
15. Neill, S. P., Hashemi, M. R., & Lewis, M. J. (2014). The role of tidal asymmetry in characterizing the tidal energy resource of Orkney. *Renewable Energy, 68,* 337–350.
16. Ohlmann, C., White, P., Washburn, L., Emery, B., Terrill, E., & Otero, M. (2007). Interpretation of coastal HF radar–derived surface currents with high-resolution drifter data. *Journal of Atmospheric and Oceanic Technology, 24*(4), 666–680.
17. Paduan, J. D., & Washburn, L. (2013). High-frequency radar observations of ocean surface currents. *Annual Review of Marine Science, 5,* 115–136.
18. Polagye, B., & Thomson, J. (2013). Tidal energy resource characterization: Methodology and field study in Admiralty Inlet, Puget Sound, WA (USA). *Proceedings of the Institution of Mechanical Engineers, Part A: Journal of Power and Energy*.
19. Prandle, D. (1991). A new view of near-shore dynamics based on observations from HF radar. *Progress in Oceanography, 27*(3), 403–438.
20. Prandle, D., & Ryder, D. K. (1985). Measurement of surface currents in Liverpool Bay by high-frequency radar. *Nature, 315,* 128–131.

21. Röhrs, J., Sperrevik, A. K., Christensen, K. Ha., Broström, G., & Breivik, Ø. (2015). Comparison of HF radar measurements with Eulerian and Lagrangian surface currents. *Ocean Dynamics*, *65*(5), 679–690.
22. Sentchev, A., Forget, P., Barbin, Y., & Yaremchuk, M. (2013). Surface circulation in the Iroise Sea (W. Brittany) from high resolution HF radar mapping. *Journal of Marine Systems, 109,* S153–S168.
23. Sentchev, A., Forget, P., & Fraunié, P. (2017). Surface current dynamics under sea breeze conditions observed by simultaneous HF radar, ADCP and drifter measurements. *Ocean Dynamics, 67*(3–4), 499–512.
24. Sentchev, A., & Yaremchuk, M. (2007). VHF radar observations of surface currents off the northern Opal coast in the eastern English Channel. *Continental Shelf Research, 27*(19), 2449–2464.
25. Sentchev, A., & Yaremchuk, M. (2016). Monitoring tidal currents with a towed ADCP system. *Ocean Dynamics, 66*(1), 119–132.
26. Stewart, R. H., & Joy, J. W. (1974). HF radio measurements of surface currents. In: *Deep Sea Research and Oceanographic Abstracts* (Vol. 21, pp. 1039–1049). Elsevier.
27. Teague, C. C., Vesecky, J. F., & Fernandez, D. M. (1997). *HF radar instruments, past to present*. *Oceanography, 10*, 40–44.
28. Thiébaut, M., & Sentchev, A. (2016). Tidal stream resource assessment in the Dover Strait (eastern English Channel). *International Journal of Marine Energy, 16,* 262–278.
29. Thiébaut, M., & Sentchev, A. (2017). Asymmetry of tidal currents off the W. Brittany coast and assessment of tidal energy resource around the Ushant Island. *Renewable Energy, 105,* 735–747.
30. Thiébaux, H. J., & Pedder, M. A. (1987). *Spatial objective analysis with applications in atmospheric science*. London: Academic Press.
31. Thomson, R. E., & Emery, W. J. (2001). *Data analysis methods in physical oceanography*. Elsevier.
32. Vennell, R. (1994). Acoustic Doppler current profiler measurements of tidal phase and amplitude in Cook Strait, New Zealand. *Continental Shelf Research, 14*(4), 353–364.
33. Yaremchuk, M., & Sentchev, A. (2009). Mapping radar-derived sea surface currents with a variational method. *Continental Shelf Research, 29*(14), 1711–1722.
34. Yaremchuk, M., & Sentchev, A. (2011). A combined EOF/variational approach for mapping radar-derived sea surface currents. *Continental Shelf Research, 31*(7), 758–768.